 CMES, vol.39, no.1, pp.49-66, 2009

Simulation of the Slow Drag of a Cylinder through a Confined Pressurized Bed of Dumbbell and Elliptically Cylindrical Granules Using the Discrete Element Method

Fuping Zhou[1], **Suresh G. Advani**[2] **and Eric D. Wetzel**[3]

Abstract: Slow drag of a cylinder through a confined, pressurized bed of granules is studied using two-dimensional discrete element method (DEM) simulations. The time-dependent total drag force experienced by the circular cylinder is calculated from the normal and tangential contact forces between the surfaces. To evaluate the role of the granule shape and the aspect ratio on the drag force, the simulation is performed for cylindrical granules, dumbbell-shaped granules, and elliptical granules of three different aspect ratios. Simulation results show that the drag in dumbbell-shaped granules is higher than that in cylindrical granules. In contrast, the drag in elliptical granules decreases as the aspect ratio increases. The flow pattern in elliptical granules is also shown to be much more irregular compared with that of cylindrical and dumbbell-shaped granules.

1 Introduction

The flow behavior of granular materials in natural and industrial systems commonly fall into two categories: surface granular flow, and confined granular flow. Surface granular flow occurs when flow takes place within a surface layer of a bed or pile of granular material. These flows are normally driven by gravity, and include chute flow [Baran, Ertas, Halsey, Grest and Lechman (2006); Pouliquen (2004); Pouliquen, Cassar, Jop, Forterre and Nicolas (2006); Silbert, Ertas, Grest, Halsey, Levine and Plimpton (2001)] and rotating drum geometry [Felix, Falk and D'Ortona (2007); Orpe and Khakhar (2007); Pohlman, Meier, Lueptow and Ottino (2006); Pohlman, Ottino and Lueptow (2006)]. In contrast, confined granular flow places the granular materials under a state of sustained high stress. Granules in confined flow can be driven by the movement of the domain boundaries or embedded

[1] ExxonMobil Upstream Research Company, 3120 Buffalo Speedway, Houston, Texas, 77098
[2] Corresponding Author: Department of Mechanical Engineering, University of Delaware, Newark, Delaware, 19716, USA. Tel: 1-302-831-8975; fax: 1-302-831-3619; Email: advani@udel.edu
[3] Army Research Laboratory, Aberdeen Proving Ground, Maryland 21005

bodies within the granular bed, such as mixing vanes. Previous experiments show that drag on a cylinder pulled through a confined granular flow is much higher than the drag on a cylinder pulled through an unconfined granular bed [Zhou, Advani and Wetzel (2004), (2005)].

Granule shape in the bed has a strong effect on granular behavior [Favier, Abbaspour-Fard and Kremmer (2001)]. Han *et al.* studied irregular particle transport in turbulent flows by coupling Lattice Boltzmann method (LBM) and the discrete element method (DEM) [Han, Feng and Owen (2007)]. Mustoe *et al.* [Mustoe and Miyata (2001)] simulated noncircular shaped particles with analytical surface representations. Desmond and Franklin [Desmond and Franklin (2006)] studied the jamming of 3D prolate granular materials, and found that the ability of long thin rods to jam into a solid-like state in response to a local perturbation depends upon both the particle aspect ratio and the container size. Using Monte Carlo simulations, Abreu *et al.* [Abreu, Tavares and Castier (2003)] demonstrated that particle aspect ratio has a strong influence on the packing of sphero-cylinders. One common approach for modeling non-spherical granules is to approximate the granules as ensembles of multiple spherical granules [Favier, Abbaspour-Fard and Kremmer (2001); Vu-Quoc, Zhang and Walton (2000)], with contact detection determined by applying spherical contact models to the granule sub-particles. In soil engineering, ellipsoidal granules have been used to represent sand. Ting *et al.* [Ting, Khwaja, Meachum and Rowell (1993)] concluded that the two-dimensional ellipse-based discrete element method (DEM) can simulate the behavior of real soils. Wang [Wang, Wang and Sheng (1999)] and Johnson [Johnson, Williams and Cook (2004)] simplified the problem by representing ellipsoidal particles using three-arc ellipse approximations.

Our previous work used a two-dimensional DEM to study the dragging of a cylinder through a confined bed of cylindrical particles [Zhou, Advani and Wetzel (2007)]. In this paper, we will simulate the two-dimensional flow behavior of dumbbell-shaped (ensemble of two cylindrical granules) granules and elliptically cylindrical granules to study the effect of irregularities and aspect ratio in confined granular flow. For compactness, we will use the term "elliptical" to describe "elliptically cylindrical" granules.

2 Approach

2.1 DEM overview

DEM is a numerical method for computing the interaction of a large number of particles such as glass beads or grains of sand, and was originally used by Cundall in 1971 for solving problems in rock mechanics [Cundall and Strack (1979)]. The

grain is treated individually with rotational and translational degrees of freedom. The granules interact when the distance separating them is less than the sum of their radii. The interaction is determined by contact and the friction laws between granules. The position $\mathbf{x}_i$ of granule with mass m_i is calculated using Newton's law by summing all forces $\mathbf{F}_{ij}$ acting on the granule at time t,

$$m_i \frac{d^2\mathbf{x}_i}{dt^2} = \sum_{j=1}^{J} \mathbf{F}_{ij} \quad . \tag{1}$$

Granule rotation is calculated as follows,

$$I_i \frac{d^2\theta_i}{dt^2} = \sum_{j=1}^{J} F_{ij}^s R_i \tag{2}$$

where I_i is the moment of inertia, and θ_i is the relative angular position, and R_i is the radius of the granule.

The most common granular shape used in discrete element simulation is a two dimensional cylindrical granule (Figure 1). The numerical model and conditions used in the present study are similar to our previous work [Zhou, Advani and Wetzel (2007)], so only the specific modifications for dumbbell shaped and elliptical granules are addressed in this paper. Note that Ting *et al.* [Ting, Khwaja, Meachum and Rowell (1993)] detected the overlap between ellipse-based granules with analytical solutions in which a quartic equation is solved to find up to four roots. Here, we detect the overlap between elliptical granules numerically as described in section IIC.

2.2 Motion of dumbbell-shaped particles

The movement of a cylinder through a packed bed of dumbbell shaped granules is shown in Figure 2. We define a dumbbell-shaped granule (Fig. 3) as two identically-sized, cylindrical sub-granules that share a single dumbbell contact point C at which no relative translational or rotational motion is allowed. The cylindrical sub-granules that comprise the granule have centers A and B at positions $\mathbf{x}_A$ and $\mathbf{x}_B$, respectively. The position of the granule is defined by the position $\mathbf{x}_C$ of the dumbbell contact point, while the granule orientation θ_C is defined by the angle of the line drawn between the centers of the two cylindrical sub-granules relative to the global coordinate system. The rate of change in position and orientation for this dumbbell-shaped granule are defined as $\dot{\mathbf{x}}_\mathbf{C}$ and $\dot{\theta}_\mathbf{C}$, respectively.

The position and velocity of sub-granules A and B are given by

$$\mathbf{x_A} = \mathbf{x_C} + \mathbf{r_{CA}} \tag{3}$$

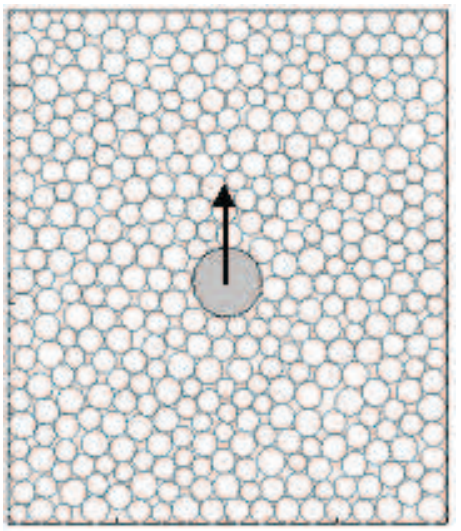

Figure 1: Two dimensional schematic of a cylinder moving relative to a packed bed of cylindrical granules.

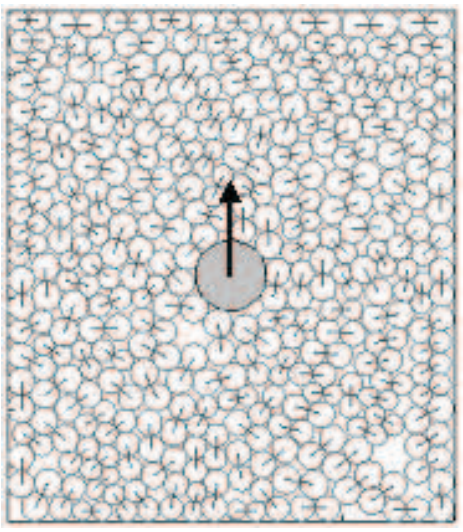

Figure 2: Two dimensional schematic of a cylinder moving relative to a packed bed of dumbbell shaped granules.

$$\mathbf{x_B} = \mathbf{x_C} + \mathbf{r_{CB}} \tag{4}$$

$$\dot{\mathbf{x}}_\mathbf{A} = \dot{\mathbf{x}}_\mathbf{C} + \dot{\theta}_C \hat{\mathbf{k}} \times \mathbf{r_{CA}} \tag{5}$$

$$\dot{\mathbf{x}}_\mathbf{B} = \dot{\mathbf{x}}_\mathbf{C} + \dot{\theta}_C \hat{\mathbf{k}} \times \mathbf{r_{CB}} \tag{6}$$

where $\mathbf{r}_{CA}$ is the vector from C to A, and $\mathbf{r}_{CB}$ is the vector from C to B.

Using these definitions of dumbbell position and orientation, as well as sub-granule position and orientation, the Hertzian non-linear spring dashpot models from Ref [Zhou, Advani and Wetzel (2007)] can be directly employed to calculate the contact forces acting on each dumbbell-shaped granule. In addition, the Coulombic frictional models from [Zhou, Advani and Wetzel (2007)] are also used to determine granule interactions.

2.3 Contact forces for elliptical granules

Movement of a cylinder across elliptically shaped granules is shown in Figure 4. Elliptical granules can impart translational and rotational forces to their neighbors through normal and tangential contacts. Contact point detection for elliptical granules is different from that of cylindrical granules.

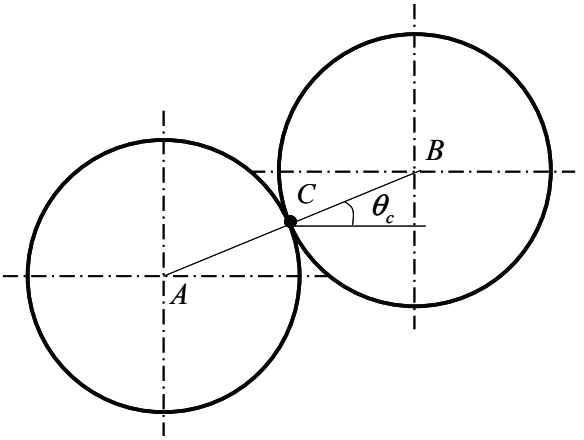

Figure 3: Dumbbell-shaped granule.

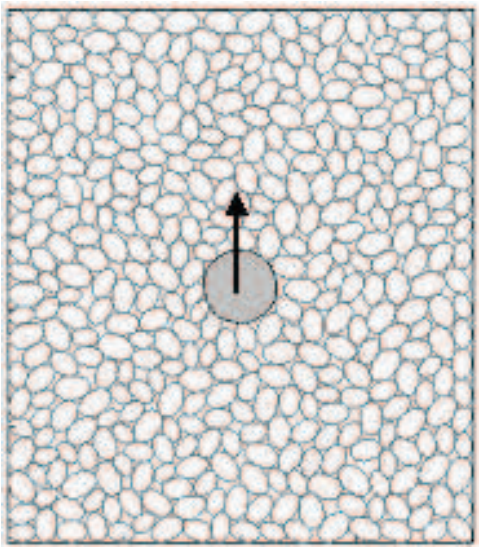

Figure 4: Two dimensional schematic of a cylinder moving relative to a packed bed of elliptical granules.

The boundary $\tilde{\mathbf{u}}$ of a two-dimensional ellipse in its local coordinate system can be defined by

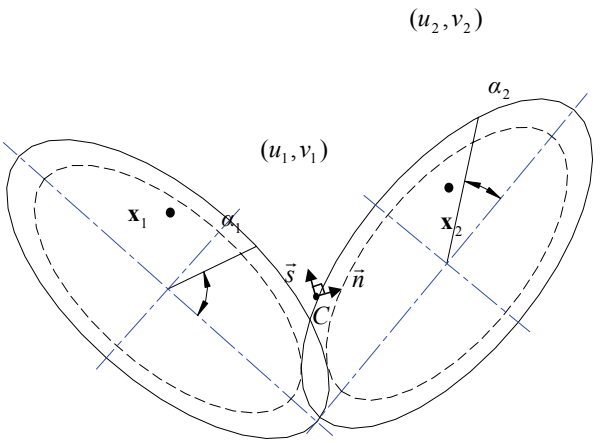

Figure 5: Contacts between two elliptical granules 1 and 2.

$$\begin{aligned} \tilde{u} &= a\cos(\alpha) \\ \tilde{v} &= b\sin(\alpha) \end{aligned} \tag{7}$$

where a and b are the major and minor semi-axis lengths, respectively, $a > b$, and α is the azimuthal angle $\alpha \in (0, 2\pi]$.

Consider two elliptical granules with centers at $\mathbf{x}_1$ and $\mathbf{x}_2$ (Fig. 5). In global coordinates, the boundary of granule 1 is given by

$$\begin{aligned} u_1 &= a_1\cos(\alpha_1)\cos(\theta_1) - b_1\sin(\alpha_1)\sin(\theta_1) + x_1 \\ v_1 &= a_1\cos(\alpha_1)\sin(\theta_1) + b_1\sin(\alpha_1)\cos(\theta_1) + y_1 \end{aligned} \tag{8}$$

where a_1, b_1, α_1, and θ_1 are the semi-axis lengths, azimuthal angle, and particle orientation for granule 1, respectively. Similarly, the boundary of granule 2 is given by

$$\begin{aligned} u_2 &= a_2\cos(\alpha_2)\cos(\theta_2) - b_2\sin(\alpha_2)\sin(\theta_2) + x_2 \\ v_2 &= a_2\cos(\alpha_2)\sin(\theta_2) + b_2\sin(\alpha_2)\cos(\theta_2) + y_2 \end{aligned} \tag{9}$$

where a_2, b_2, α_2, and θ_2 are the semi-axis lengths, azimuthal angle, and particle orientation for granule 2, respectively.

In the local coordinate system of granule 2, the boundary of granule 1 is given by

$$\begin{aligned} \tilde{u}_{12} &= a_1\cos(\alpha_1)\cos(\theta_1-\theta_2) - b_1\sin(\alpha_1)\sin(\theta_1-\theta_2) + \cos(\theta_2)(x_1-x_2) + \sin(\theta_2)(y_1-y_2) \\ \tilde{v}_{12} &= a_1\cos(\alpha_1)\sin(\theta_1-\theta_2) + b_1\sin(\alpha_1)\cos(\theta_1-\theta_2) - \sin(\theta_2)(x_1-x_2) + \cos(\theta_2)(y_1-y_2) \end{aligned}$$

(10)

We can define the function $G(\tilde{u}_{12}, \tilde{v}_{12})$ as

$$G(\tilde{u}_{12}, \tilde{v}_{12}) = \frac{(\tilde{u}_{12})^2}{a_2^2} + \frac{(\tilde{v}_{12})^2}{b_2^2} - 1 \tag{11}$$

where a_2 and b_2 are the semi-axis lengths of granule 2. Points $(\tilde{u}_{12}, \tilde{v}_{12})$ on granule 1 are on the boundary of granule 2 if $G(\tilde{u}_{12}, \tilde{v}_{12})$=0, are outside of granule 2 if $G(\tilde{u}_{12}, \tilde{v}_{12})$>0, and are inside of granule 2 if $G(\tilde{u}_{12}, \tilde{v}_{12})$<0. Therefore, if $G(\tilde{u}_{12}, \tilde{v}_{12})$<0, overlap exists between the granules.

The overlap δ between granules can be calculated by

$$\delta = \sqrt{(u_2 - u_1)^2 + (v_2 - v_1)^2}. \tag{12}$$

The normal and tangential unit vector at the contact point C (Fig. 5) can be calculated as,

$$\begin{aligned} \hat{\mathbf{n}} &= \left((u_2 - u_1)\hat{\mathbf{i}} + (v_2 - v_1)\hat{\mathbf{j}} \right) / \delta \\ \hat{\mathbf{s}} &= \left(-(v_2 - v_1)\hat{\mathbf{i}} + (u_2 - u_1)\hat{\mathbf{j}} \right) / \delta \end{aligned} . \tag{13}$$

The relative velocity $\dot{\mathbf{x}}_\mathbf{c}$ of granule 1 with respect to granule 2 at their contact point is

$$\Delta\dot{\mathbf{x}}_c = \dot{\mathbf{x}}_2 + \dot{\theta}_2\hat{\mathbf{k}} \times \mathbf{r}_2 - (\dot{\mathbf{x}}_1 + \dot{\theta}_1\hat{\mathbf{k}} \times \mathbf{r}_1). \tag{14}$$

The normal direction component of relative velocity is given by

$$\Delta\dot{x}_{cn} = (\dot{\mathbf{x}}_2 + \dot{\theta}_2\hat{\mathbf{k}} \times \mathbf{r}_2 - (\dot{\mathbf{x}}_1 + \dot{\theta}_1\hat{\mathbf{k}} \times \mathbf{r}_1)) \cdot \hat{\mathbf{n}}. \tag{15}$$

while the tangential component of the relative velocity is given by

$$\Delta\dot{x}_{cs} = (\dot{\mathbf{x}}_2 + \dot{\theta}_2\hat{\mathbf{k}} \times \mathbf{r}_2 - (\dot{\mathbf{x}}_1 + \dot{\theta}_1\hat{\mathbf{k}} \times \mathbf{r}_1)) \cdot \hat{\mathbf{s}}. \tag{16}$$

Figure 6 depicts the contact between the wall and a granule. The coordinates of the contact point (x_c, y_c) between a granule and the right wall can be calculated as

$$\begin{aligned} x_c &= x_1 + w \\ y_c &= y_1 + \frac{\left(b_1^2 - a_1^2\right)\sin(\theta_1)\cos(\theta_1)}{a_1^2\sin^2(\theta_1) + b_1^2\cos^2(\theta_1)} w \end{aligned} \tag{17}$$

where $w = x_w - x_1$ and x_w is the x-coordinate of the wall.

Coordinates of a contact point between granules and other walls can be calculated in a similar manner. The contact and friction forces between granules and walls can be calculated via Hertz contact law and Coulombic friction laws, respectively, as discussed in [Zhou, Advani and Wetzel (2007)].

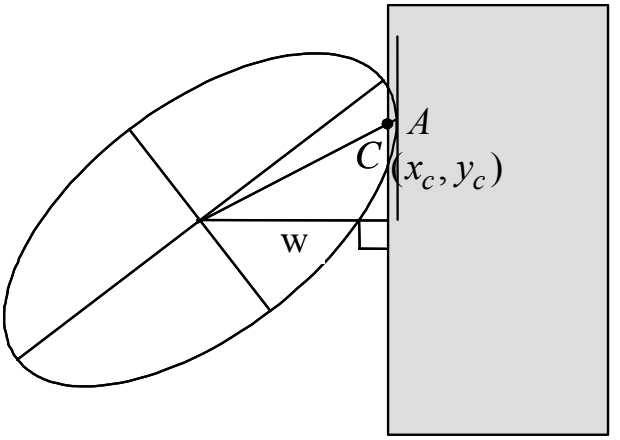

Figure 6: Contact between wall and a granule.

3 Results

3.1 Parameter description and initial conditions

Simulations are performed for the slow drag of a rigid cylinder of diameter D_c through a packed bed of two-dimensional granules of diameter D_g, confined within a fixed-wall container with width W and height H. The number of granules is N_g, and the cylinder is pulled at a velocity $\dot{s}$, generating a drag force F_d as a function of cylinder position s. The volume fraction V_f of granules in the container is defined as

$$V_f = \frac{V_g}{V_w - V_c}, \tag{18}$$

where V_g is the total volume of all granules, V_w is the volume of the container, and V_c is the volume of the cylinder. Unless otherwise specified, the parameters used in all simulations are: cylinder diameter D_c = 3.175mm, cylinder velocity $\dot{s}$ = 2 m/s, container width W = 20, granule volume fraction V_f =0.84, granule density $\rho = 3.9 \times 10^3$ kg/m^3, and number of granules N_g = 400.

The shape of the elliptical granules is represented by the aspect ratio $\lambda = a/b$. The size of the elliptical granules is summarized using a "volume diameter", which is the diameter of a cylindrical particle having the same volume as the elliptical particle, or $\sqrt{ab}$. Since uniform grain size will introduce ordering effects, the granules were allowed to randomly assume a diameter between +20% and -20% of their average diameter. For dumbbell-shaped particles, a representative volume diameter D_g is defined so that each sphere in the dumbbell has a diameter of $\sqrt{2}D_g/2$.

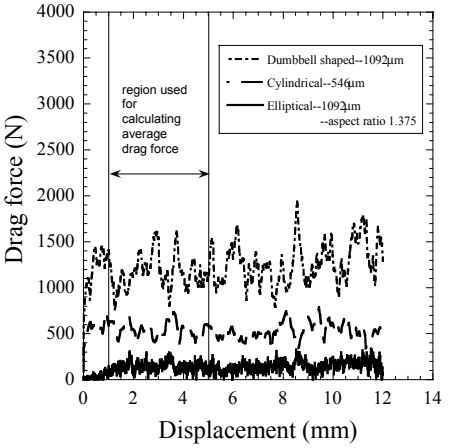

Figure 7: Total drag force experienced by the cylinder as it moves through the packed bed of granules. Results are averaged at each displacement location over 5 simulations.

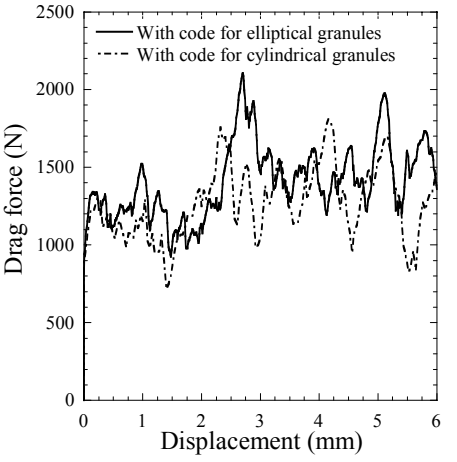

Figure 8: Comparison of drag force calculations for cylindrical code, and elliptical code for case of =1.

Figure 7 shows the general behavior of drag in cylindrical, dumbbell-shaped, and elliptical granules. During a single simulation, the instantaneous drag force on the cylinder varies as the cylinder moves through the confined bed. To reduce variability, a series of five simulations are performed for each condition. Each of these simulations has identical parametric conditions, but random initial granule positions. The average force calculated at each position s over the five simulations is reported in Figure 7, and all subsequent results. The overall average drag force is then characterized as the average drag force over the cylinder as it is displaced from 1 mm to 5 mm (Fig. 7). As discussed in [Zhou, Advani and Wetzel (2007)], solution convergence is demonstrated by reducing the simulation time step until the average drag force converges to a consistent value.

3.2 Numerical validation

Figure 8 compares the simulation results for the elliptical granule code, for the case of λ=1, with the simulation results for the cylindrical code from [Zhou, Advani and Wetzel (2007)]. In this calculation, D_g = 1092. The average drag forces and standard deviations for the elliptical and cylindrical codes are 1405 N and 17%, and 1295 N and 18%, respectively. The differences in these drag force values are within the standard deviation of the drag force itself, confirming the validity of the elliptical code in the limit of a cylindrical granule.

3.3 Effect of granule shape

To study the effect of granular shape on the drag force, simulations were conducted for the granule shapes and sizes shown in Table 1. Simulations c_1 and d_1 compare cylindrical and dumbbell-shaped particles, for the case of equal effective particle diameters. Cases c_1 and e_1 compare cylindrical and elliptical particles, for the case of equal effective particle diameters. Cases c_2, e_1, e_2, and e_3 compare elliptical particles of equal granule size and increasing aspect ratio.

Table 1: Granules shapes used for the simulations.

Symbol	Shape	Aspect ratio λ	Granule size D_g (μm)
c_1	Cylindrical	1	1092
d_1	Dumbbell-shaped	2	1092
c_2	Cylindrical	1	772
e_1	Elliptical	1.125	1092
e_2	Elliptical	1.25	1092
e_3	Elliptical	1.375	1092

The visualization of DEM results are shown in Figs. 9-12. To characterize the granular flow, one cluster of granules in front of the cylinder is shaded. Figure 9 shows three snapshots at different displacements during the upward movement of the cylinder for three different granule geometries (Table 1). To further visualize the overall flow pattern, Fig. 10 represents the same snapshots as Fig. 9, but a different coloration pattern is used to distinguish the granular layers. No dramatic differences in qualitative particle flow behavior are evident for these three different particle shapes and sizes.

Figure 11 shows three snapshots of the drag in elliptical granules with aspect ratios of 1.125 (e_1), 1.25 (e_2) and 1.375 (e_3) respectively (Table 1). The average size of the elliptical granules is the same as that of cylindrical granules from simulation c_1. To further visualize the overall flow pattern, Fig. 12 represents the same snapshots as Fig. 11, but a different coloration pattern is used to distinguish the granular layers. Comparing cases c_1, e_1, and e_2, little qualitative difference in flow patterns is evident. However, case e_3 shows a significantly large mixing zone, with more randomness imparted to the granular bed at the later stages of the simulation.

Figure 13 compares the drag force calculated from the simulations of the granules listed in Table 1. Comparing c_1 and d_1, dumbbell-shaped particles exhibit less drag than cylindrical particles of equal effective diameter. Comparing d_1 and c_2, dumbbell-shaped particles show significantly higher drag than cylindrical particles

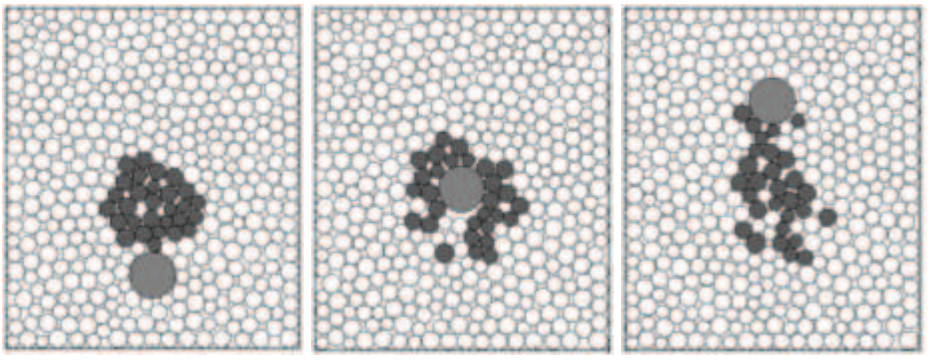

s = 0mm s = 6mm s = 12mm

(a) simulation c_1

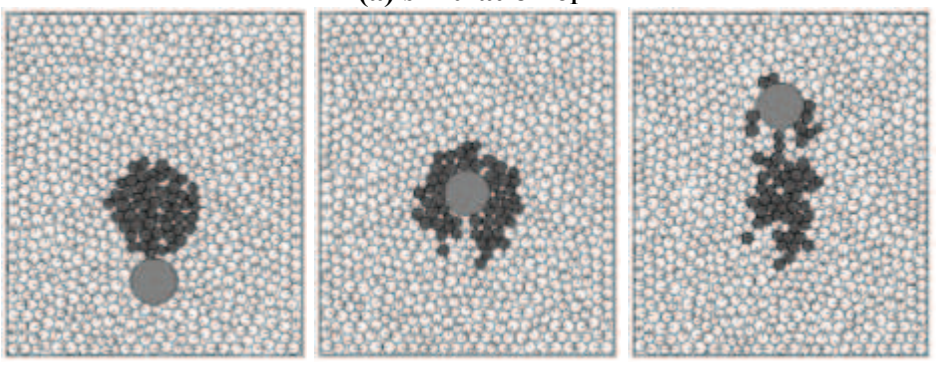

s = 0mm s = 6mm s = 12mm

(b) simulation d_1

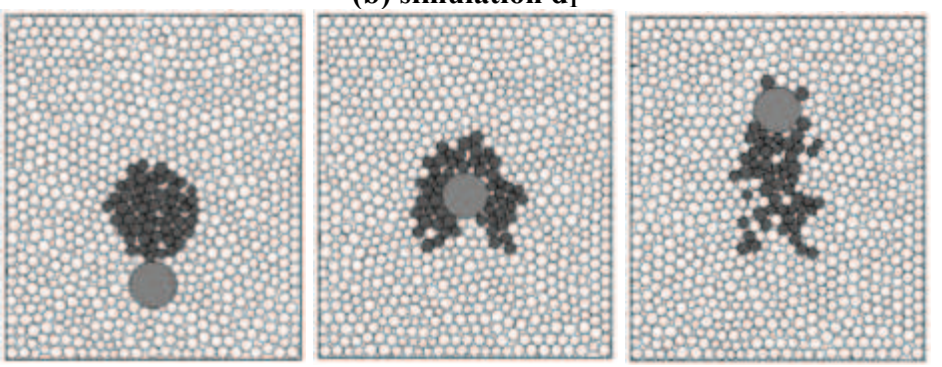

s = 0mm s = 6mm s = 12mm

(c) simulation c_2

Figure 9: Snapshots at identical cylinder displacements during dragging of a cylinder through a bed of cylindrical or dumbbell-shaped granules for cases c_1, d_1, and c_2 as specified in Table 1. The cluster of granules in front of the cylinder are labeled and tracked during the motion of the cylinder.

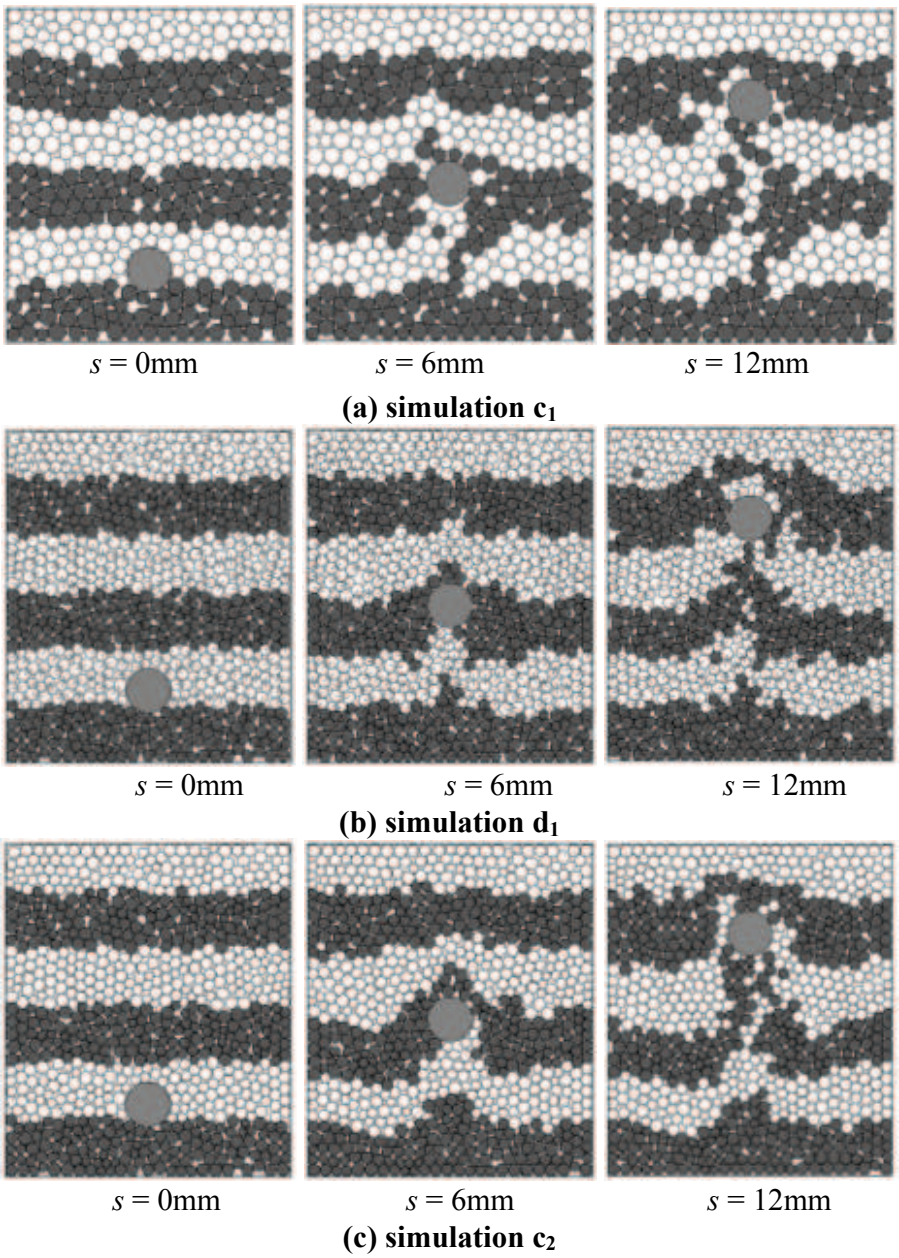

Figure 10: Snapshots at identical cylinder displacements during dragging of a cylinder through a bed of cylindrical or dumbbell-shaped granules for cases c_1, d_1, and c_2 as specified in Table 1. The results are identical to those shown in Fig. 9, but a different coloration scheme is used to mark the granules.

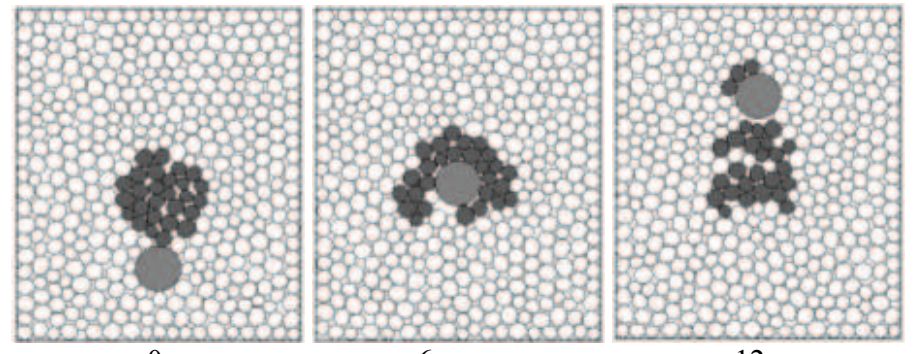

s = 0mm s = 6mm s = 12mm

(a) simulation e_1

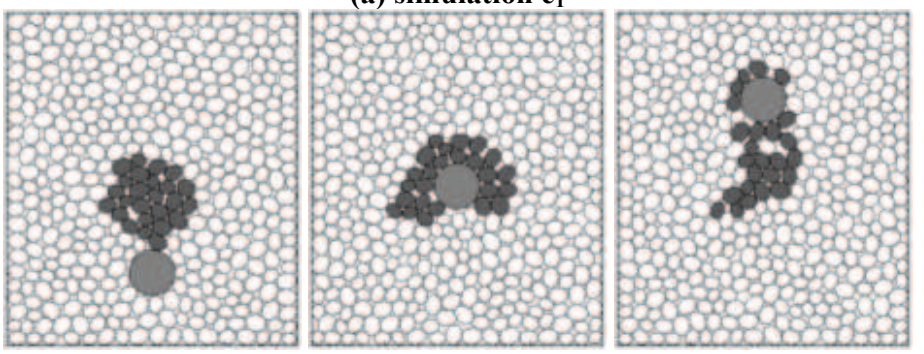

s = 0mm s = 6mm s = 12mm

(b) simulation e_2

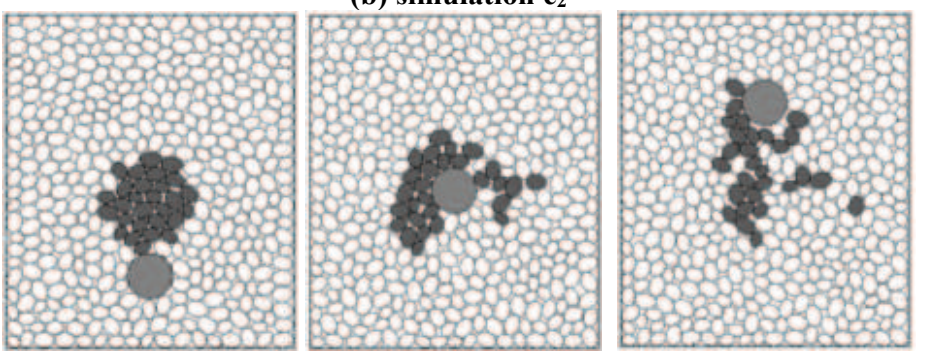

s = 0mm s = 6mm s = 12mm

(c) simulation e_3

Figure 11: Snapshots at identical cylinder displacements during motion of a cylinder through a bed of elliptical granules for cases e_1, e_2, and e_3 as specified in Table 1. The cluster of granules in front of the cylinder is tracked during the motion of the cylinder.

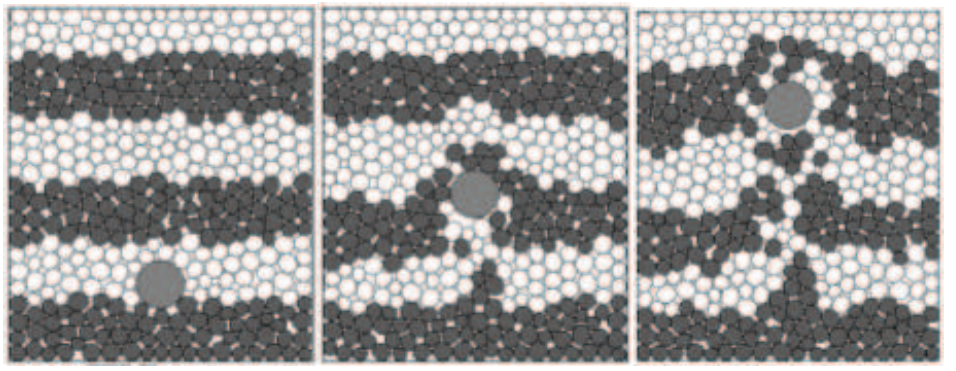

s = 0mm s = 6mm s = 12mm

(a) simulation e_1

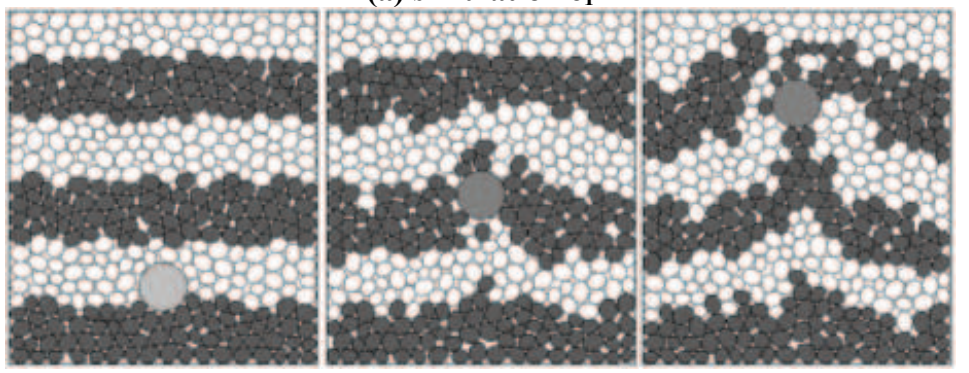

s = 0mm s = 6mm s = 12mm

(b) simulation e_2

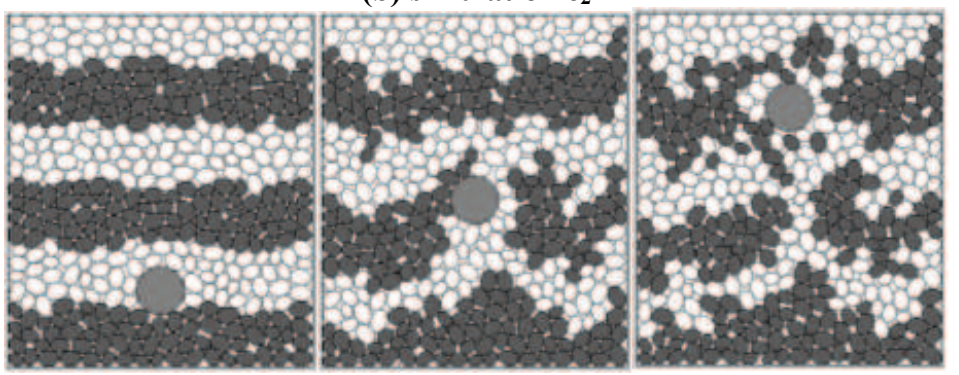

s = 0mm s = 6mm s = 12mm

(c) simulation e_3

Figure 12: Snapshots at identical cylinder displacements during motion of a cylinder through a bed of elliptical granules for cases e_1, e_2, and e_3 as specified in Table 1. The results are identical to those shown in Fig. 11, but a different coloration scheme is used to mark the granules.

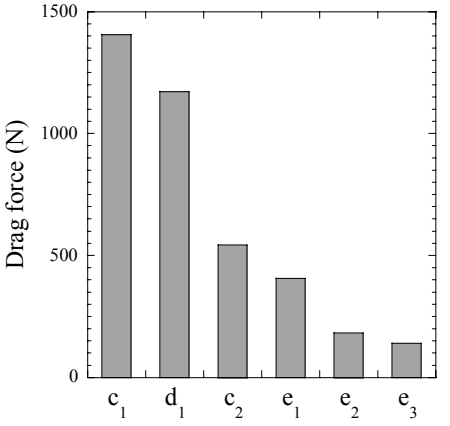

Figure 13: Average drag force on the cylinder as it is displaced through a granular bed of cylindrical, dumbbell shaped and elliptical particles with parameters specified in Table 1.

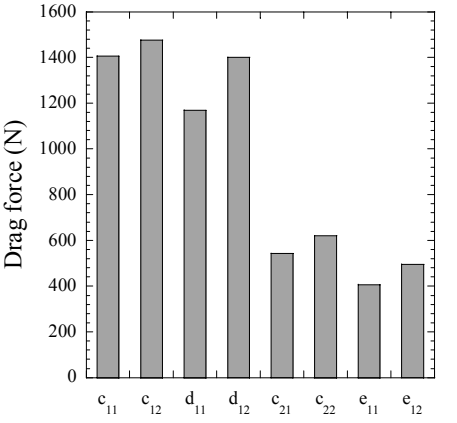

Figure 14: The influence of granule density on the drag force. All the parameters are specified in Table 2.

if the diameter of the two sub-particles in the dumbbell is equal to the cylinder diameter. Comparing c_1 and e_1, there is a remarkable drop in drag force when the granules are made slightly elliptical. This drop in drag force could result from the ability of elongated particles to align with the particle flow direction during drag. Further increases in aspect ratio for cases e_2 and e_3 result in further drops in the calculated drag force.

3.4 Effect of particle density

Previous work shows that the compaction forces and friction contribute significantly to the drag force [Zhou, Advani and Wetzel (2007)]. To examine the role of gravity, drag simulations were performed for cylindrical, dumbbell-shaped, and elliptical granules for cases of two different granule density values, as shown in Table 2. The results are shown in Fig. 14. Although the density has increased by a factor of 10, the maximum change in drag force is 21.8%**.** This result indicates that, within the bounds of our simulations, momentum effects are relatively insignificant relative to frictional and compaction forces. This conclusion is also supported by previous simulations under similar conditions and have also shown that there is little effect of velocity on drag behavior [Zhou, Advani and Wetzel (2007)] .

Table 2: Values used for granule size, shape and density to examine the role of density on the drag force.

Symbol	Shape	Aspect ratio λ	Granule size D_g (μm)	Granule density (kg/m^3)
c_{11}	Cylindrical	1	1092	3.9×10^3
c_{12}	Cylindrical	1	1092	3.9×10^4
d_{11}	Dumbbell shaped	2	1092	3.9×10^3
d_{12}	Dumbbell shaped	2	1092	3.9×10^4
c_{21}	Cylindrical	1	772	3.9×10^3
c_{22}	Cylindrical	1	772	3.9×10^4
e_{11}	Elliptical	1.125	1092	3.9×10^3
e_{12}	Elliptical	1.125	1092	3.9×10^4

4 Conclusions

Discrete element method simulations were used to calculate the drag force on a cylinder moving through a compacted bed of granules of different shapes and sizes. A non-linear spring dashpot model based on Hertz contact theory, and Coulombic frictional rules was used to describe granule-granule interactions. Results show that the drag force in dumbbell-shaped granules is higher than that in cylindrical granules of equivalent volume. However, the drag in dumbbell-shaped granules is higher than in cylindrical granules when the cylinder diameter is equal to the diameter of the two sub-particles comprising the dumbbell. For elliptical granules, the drag force decreases with granule aspect ratio. Visualization results demonstrate that the flow pattern in elliptical granules with an aspect ratio of 1.375 is much more irregular than those of lower aspect ratios. These results demonstrate that the granule shape strongly influences the drag force experienced by an object that is displaced through a confined, pressurized bed of granular materials.

Acknowledgement: The support of the project from the Army Research Laboratory is gratefully acknowledged. A discrete simulation code downloaded from the website of Dr. Carl E. Wassgren was the starting point in the development of the simulation code for the presented work.

References

Abreu, C.R.A.; Tavares, F.W.; Castier, M. (2003): Influence of particle shape on the packing and on the segregation of spherocylinders via Monte Carlo simulations, *Powder Technol.*, vol. 134, pp. 167-180.

Baran, O.; Ertas, D.; Halsey, T. C.; Grest, G. S.; Lechman, J. B. (2006): Ve-

locity correlations in dense gravity-driven granular chute flow, *Physical Review E*, vol. 74.

Cundall, P. A.; Strack, O.D.L. (1979):A discrete numerical-model for granular assemblies: *Geotechnique*, vol. 29, pp. 47-65.

Desmond, K.Franklin, S. V. (2006):Jamming of three-dimensional prolate granular materials, *Physical Review E*, vol. 73, 031306.

Favier, JF; Abbaspour-Fard, M.H.; Kremmer, M. (2001): Modeling nonspherical particles using multisphere discrete elements, *J. ENG. MECH-ASCE*, vol. 127, pp. 971-977.

Felix, G.; Falk, V.D.; Ortona, U. (2007): Granular flows in a rotating drum: the scaling law between velocity and thickness of the flow, *European Physical Journal E*, vol. 22, pp. 25-31.

Han, K.; Feng, Y.T.; Owen, D.R.J. (2007): Numerical simulations of irregular particle transport in turbulent flows using coupled LBM-DEM, *CMES: Computer Modeling in Engineering & Sciences*, vol. 18, pp. 87-100.

Johnson, S; Williams, J.R.; Cook, B. (2004): Contact resolution algorithm for an ellipsoid approximation for discrete element modeling, *Eng. Computation*, vol. 21, pp. 215-234.

Mustoe, G.G.W.; Miyata, M. (2001): Material flow analyses of noncircular-shaped granular media using discrete element methods, *Journal of Engineering Mechanics-Asce*, vol. 127, pp. 1017-1026.

Orpe, A.V.; Khakhar, D.V. (2007): Rheology of surface granular flows, *Journal of Fluid Mechanics*, vol. 571, pp. 1-32.

Pohlman, N.A.; Meier, S.W.; Lueptow, R.M.; Ottino, J.M. (2006): Surface velocity in three-dimensional granular tumblers, *Journal of Fluid Mechanics*, vol. 560, pp. 355-368.

Pohlman, N.A.; Ottino, J.M.; Lueptow, R.M. (2006): End-wall effects in granular tumblers: From quasi-two-dimensional flow to three-dimensional flow, *Physical Review E*, vol. 74, 031305.

Pouliquen, O. (2004): Velocity correlations in dense granular flows, *Physical Review Letters*, vol. 93, 248001.

Pouliquen, O.; Cassar, C.; Jop, P.; Forterre, Y.; Nicolas, M. (2006): Flow of dense granular material: towards simple constitutive laws, *Journal of Statistical Mechanics-Theory and Experiment*, P07020.

Silbert, L.E.; Ertas, D.; Grest, G.S.; Halsey, T.C.; Levine, D.; Plimpton, S.J. (2001): Granular flow down an inclined plane: Bagnold scaling and rheology, *Physical Review E*, vol. 64, 051302.

Ting, J.M.; Khwaja, M.; Meachum, L.R.; Rowell, J.D. (1993): An ellipse-based discrete element model for granular-materials, *Int. J. Numer. Anal. Met.*, vol. 17, pp. 603-623.

Vu-Quoc, L; Zhang, X.; Walton, O.R. (2000): A 3-D discrete-element method for dry granular flows of ellipsoidal particles, *Comput. Method Appl. M.*, vol. 187, pp. 483-528.

Wang, C.Y.; Wang, C.F.; Sheng, J.P. (1999): A packing generation scheme for the granular assemblies with 3D ellipsoidal particles, *Int. J. Numer. Anal. Met.*, vol. 23, pp. 815-828.

Zhou, F.P.; Advani, S.G.; Wetzel, E.D. (2004): Slow drag in granular materials under high pressure, *Phys. Rev. E*, vol. 69, 061306.

Zhou, F.P.; Advani, S.G.; Wetzel, E.D. (2005): Slow drag in polydisperse granular mixtures under high pressure, *Physical Review E*, vol. 71, 061304.

Zhou, F.P.; Advani, S.G.; Wetzel, E.D. (2007): Simulation of slowly dragging a cylinder through a confined pressurized bed of granular materials using the discrete element method, *Physics of Fluids*, vol. 19, 013301.